CRUSTAL AND UPPER-MANTLE *P*- AND *S*-VELOCITY STRUCTURE IN CENTRAL AND SOUTHERN ASIA FROM JOINT BODY- AND SURFACE-WAVE INVERSION

Delaine Reiter[1] and William Rodi[2]

Weston Geophysical Corporation[1] and Earth Resources Laboratory, Massachusetts Institute of Technology[2]

Sponsored by Air Force Research Laboratory

Contract No. FA8718-04-C-0027

ABSTRACT

Accurate travel-time predictions for regional seismic phases are essential for locating small seismic events with the accuracy needed for nuclear monitoring decisions. Travel times calculated through 3D Earth models have the best chance of achieving acceptable prediction errors, if the models are constrained by sufficient data. With this motivation, we have developed a joint body-wave/surface-wave inversion method to derive self-consistent 3D *P* and *S* velocity models for the crust and upper mantle. For body waves, our approach employs 3D finite-difference ray tracing to calculate first-arrival travel times through a 3D velocity model. Modeling of surface-wave dispersion is done using a two-step procedure. In the first step we apply 1D dispersion modeling to the velocity-depth profile at each point of a latitude/longitude grid to calculate phase- and group-velocity dispersion curves. The second step employs 2D finite-difference ray tracing to the resulting phase-velocity maps, period by period, and then integrates the group-velocity maps along the derived ray paths to obtain group delays. The use of 2D ray tracing accounts approximately for the non-great-circle propagation of surface waves in 3D Earth structures.

Our inversion approach follows these procedures in reverse. For surface waves, 2D tomography is applied to fit group-velocity maps to observed group delays along particular source-receiver paths, and then a 1D inversion technique is applied to the resulting group-velocity dispersion curve for each geographic grid point to determine an updated *S*-wave velocity-depth profile for the point. For body waves, 3D tomography is applied directly to the first-arrival travel-time residuals for observed source-receiver pairs to update the *P*-wave velocity model. An important element of our inversion approach, which serves to couple the body-wave and surface-wave problems more tightly and accommodate their differing spatial sensitivities to Earth structure, is the use of prior velocity constraints in each inversion step, determined from bounds on Poisson's ratio and the velocities themselves as a function of depth and tectonic regime.

To date, we have developed a basic version of our modeling and inversion procedures and have begun to apply them to a large region covering southern and central Asia, with the goal of determining crustal and upper-mantle structure to a depth of approximately 400 km. The surface-wave dispersion database includes group-velocity measurements provided by groups at the University of Colorado and Lawrence Livermore National Laboratory. Body-wave travel times are collected from the Engdahl, van der Hilst and Buland, EHB (1998) bulletin, screened to include first-arrival times for regional source-receiver distances and shallow event depths. Our initial model for the region is a hybrid of the CRUST2.0 3D model of crust and lid velocities (Bassin et al., 2000) and the global 1D AK135 model. In this paper we show results from the first exercise of our approach, in which we derive *P* and *S* velocity models independently from body and surface waves, respectively. This exercise allows us to determine whether the data sets and our assumed velocity and Poison's ratio constraints are all mutually consistent.

OBJECTIVES

The development and validation of accurate 3D velocity models of the crust and upper mantle for regions of nuclear monitoring interest remains a important goal for the Air Force Technical Applications Center (AFTAC). Systematic biases caused by inadequately modeled Earth structures cause errors in the estimation of geophysical parameters such as the travel times and amplitudes of regional seismic phases. More accurate and reliable estimates of these quantities (especially in aseismic regions) will improve nuclear monitoring efforts to detect, locate and discriminate regional events. Therefore, we have developed a joint 3D inversion technique that incorporates both compressional-wave travel times and Rayleigh-wave group velocity measurements to determine the full *P* and *S* velocity structure of the crust and upper mantle.

In this paper we report on the application of the first iteration of our inversion technique to data from the broad region shown in Figure 1. This region, extending from 10-50°N and 40-110°E, covers some of the most tectonically complex areas on Earth.

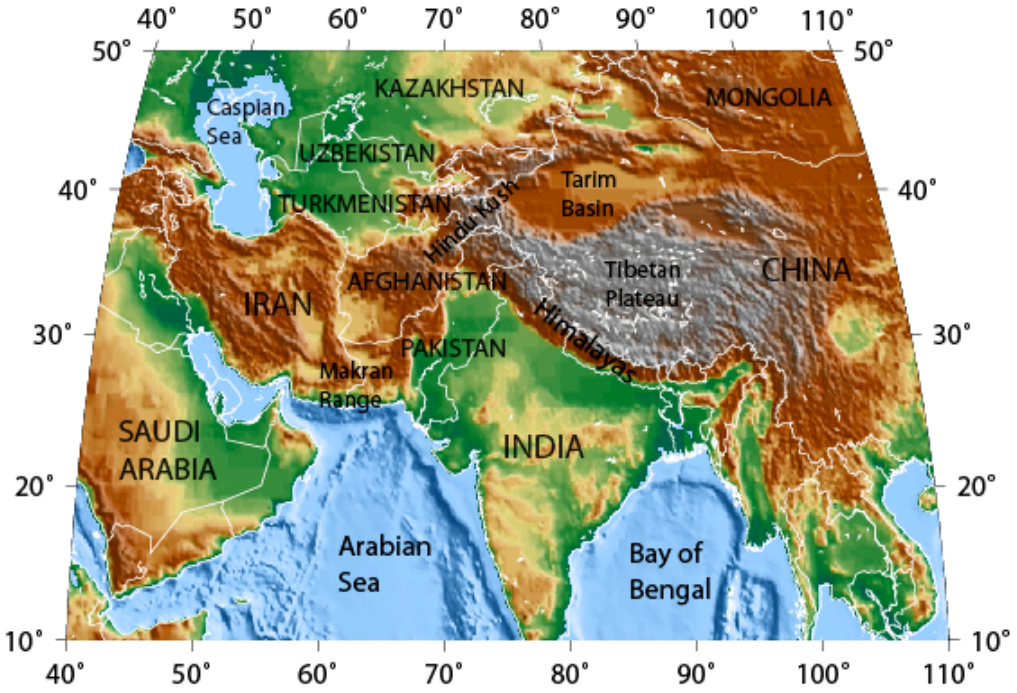

Figure 1. Topographic map of study region, which encompasses most of central and southern Asia, as well as portions of the Middle East.

RESEARCH ACCOMPLISHED

Joint Inversion Approach

The algorithms we are developing perform a joint, nonlinear inversion of body-wave travel times and surface-wave group delays to obtain fully 3D regional models of the crust and upper mantle. Problem nonlinearity is handled by iterating over linearized inversion steps, with the aid of finite-difference ray tracing techniques to perform the necessary forward modeling in the updated Earth model at each iteration step.

At each step of the iteration, we perform linearized body-wave and surface-wave inversion as separate procedures. The body-wave data, comprising only first-arrival *P*-wave times, are used to update the P velocity model (*Vp*). The surface-wave dispersion data are used to update the *S*-wave model (*Vs*), ignoring the small dependence of Rayleigh wave dispersion on P velocity. This sequential approach allows us to avoid some of the pitfalls associated with large simultaneous inverse problems. The separate inversions are coupled, however, through the prior information applied to the velocity functions.

The prior information used in each linearized inversion is of two types. First, we apply constraints on the size and spatial smoothness of velocity perturbations using a standard Tikhonov regularization approach (Tikhonov and Arsenin, 1977). The Tikhonov stabilizing functional in our case is based on a geo-statistical formulation whereby a prior variance and horizontal and vertical correlation distances are used in lieu of a simple regularization parameter (Rodi et al., 2005). The second form of prior information consists of upper and lower bounds on the *P* and *S* velocities, which are allowed to vary with depth and tectonic regime. The velocity bounds are determined in part from bounds on Poisson's ratio. Figure 2 illustrates this concept. The green six-sided admissible region in *Vp*-*Vs* space follows from constraints that might be appropriate for a point in the upper mantle: 7.7 <= *Vp* <= 8.4 km/s, 4.2 <= *Vs* <= 4.7 km/s, and Poisson's ratio (σ) between 0.25 and 0.30. If the current model velocities are 8.20 and 4.55 (black circle), the body-wave inversion would use the *Vp* bounds indicated by the horizontal line, while the surface-wave inversion would use the *Vs* bounds indicated by the vertical line. The Poisson's ratio constraints, in particular, couple the body-wave and surface-wave inversions in a way that ensures consistency between the *P* and *S* velocity models.

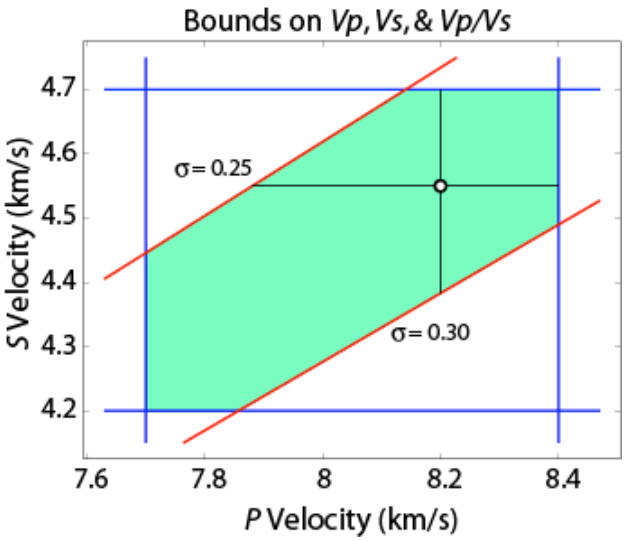

Figure 2. Illustration of the inversion bounds strategy for *Vp* and *Vs* for a sample point in the upper mantle. The upper and lower bounds on *Vp*, *Vs* and Poisson's ratio are allowed to vary with depth and tectonic regime.

To date, we have performed only the first step of the nonlinear iteration, using a 3D Earth model for the initial (reference) model. This paper presents the results of this first step and a preliminary analysis of the consistency between the body-wave and surface-wave data sets. This is an essential step toward the difficult goal of reconciling these disparate data sets, which constrain different aspects of the Earth's seismic structure.

In the next sections we present details on the travel-time and group-velocity dispersion data sets used in our inversion, followed by details and results of the inversion procedure.

Body-wave (Travel-Time) and Surface-Wave (Rayleigh Dispersion) Data Sets

Compressional-wave Travel-Time Database: The travel times we use in the *P*-wave tomography are taken from the EHB bulletin (Engdahl et al., 1998). We extracted arrivals from 1988-2004 having event and station locations within

0-60°N, 30-120°N and event depths between 0-200 km, including only first-arriving phases denoted *Pg*, *Pb* or *Pn* and which were defining phases for the EHB locations. To ensure small epicentral mislocations in the events, we required the secondary azimuth gap for a given event to be less than or equal to 130º (Bondár, Meyers, et al., 2004) and the number of teleseismic arrivals to be at least 15. The data set satisfying these criteria comprised 124,080 arrivals from 6,079 events and 735 stations.

We compressed this data set by forming summary events on a regular grid having 0.5-degree spacing in latitude and longitude and containing 13 nodes in depth between 0 and 200 km, with the depth spacing per node increasing from 5 to 20 km. For each summary-event node and each station/phase type, a summary travel-time residual (relative to the AK135 Earth model) was formed by averaging the individual residuals for the events near that node. Following this compression, stations containing fewer than 25 arrivals were dropped from the data set. The use of summary events acknowledges the redundant sensitivity of individual data to the Earth model (which is on a 1-degree grid) and, combined with the station-dropping rule, reduces the ray-tracing requirements for the inversion substantially.

The final database used in the body-wave tomography contained 76,355 arrivals for 2,998 summary events and 438 stations. The data spanned epicentral distances to 18.7 degrees, and the travel-time residuals (relative to AK135) ranged from -8.0 to 8.8 s with a root-mean-square (RMS) error of 2.5 s. The path coverage for the travel-time database is shown in Figure 2; it demonstrates that we have excellent coverage for nearly our entire study region, with the exception of the eastern tip of Saudi Arabia, where there is low seismicity and a paucity of station coverage.

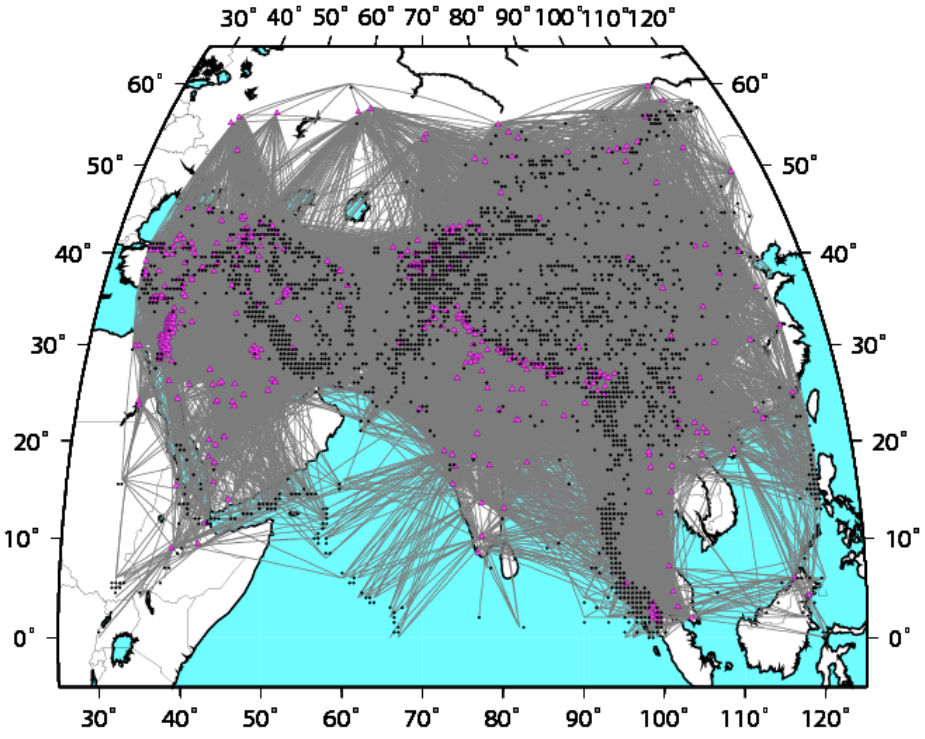

Figure 3. Path coverage for the summary-event *P*-wave travel-time data set, displayed with great-circle rays between event and station location. Purple triangles represent stations, and black dots are the summary-event locations.

Surface-wave Dispersion Database: The surface-wave dispersion database was collected from several sources, but primarily consists of measurements made by the University of Colorado at Boulder (CUB) group (Ritzwoller and Levshin, 1998) and the Lawrence Livermore National Laboratory (Pasyanos, pers. comm.). Some measurements in the region were also made by the Weston Geophysical internal group. To eliminate potential outliers in the data set, we performed a period-by-period grooming of the data, in which we retained a group velocity measurement if it was within two standard deviations of the mean group velocity for that period. This exercise resulted in a database of

61,200 fundamental-mode Rayleigh group velocity picks, for periods of T = 10-16, 18, 20, 25, 30, 35, 40, 50, 60, 70, 80, 90, 100, 120, 125 and 150 seconds. A depiction of the great-circle path coverage over our study region is shown in Figure 4. The 'footprint' or overall coverage of this data set is slightly smaller in geographical extent than that of the body-wave travel-time data set, which will become more apparent in the final inversion results. We plan to increase our group velocity data coverage to match that of the travel-time database for our final inversion runs.

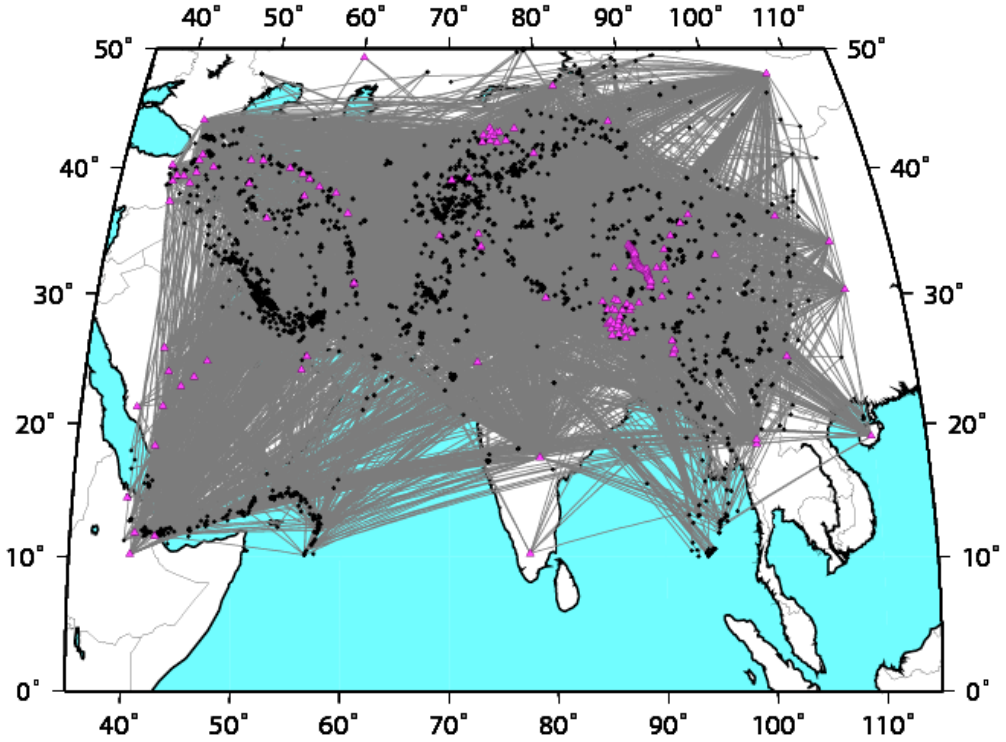

Figure 4. Path coverage for the surface-wave dispersion data set, depicted with great-circle rays between event and station locations. Purple triangles represent stations, and black dots are the event locations.

Initial Model

The initial Earth model we used for both the body-wave and surface-wave tomographies is a composite 3D model consisting of the CRUST2.0 model (Bassin et al., 2000) for the crust and the 1D AK1355 reference model (Kennett et al., 1995) for the mantle. The CRUST2.0 *Pn* velocities were ignored in favor of the AK135 velocities (Vp = 8.04 km/s, Vs = 4.48 km/s at the top of the mantle). However, the CRUST2.0 variable Moho depth was retained and accommodated by vertical compression or extension of the AK135 mantle thickness to a depth of 210 km.

A first attempt at deriving realistic velocity bounds was done as follows. First, we assigned nominal bounds for each layer of the crust based on the velocity values occurring in CRUST2.0, but not attempting to cover the entire variation in CRUST2.0 velocities. We set nominal bounds for depth-dependent mantle velocities to be the AK135 values plus or minus a fixed amount (±0.2, for *P* velocity, and ±0.1 for *S* velocity). Table 1 shows these nominal bounds, including ones chosen for specific Poisson's ratio. Second, we modified the nominal bounds on velocity to vary with the tectonic regimes assigned in CRUST2.0. Namely, the admissible range of velocities for a given regime was expanded to include (with an additional buffer) the highest and lowest values that occur (worldwide) in that regime. This exercise recognized only the major regimes identified in CRUST2.0 with leading letters A-Z (e.g., "Platform," "Archean," "Proterozoic," "extended crust"). The resulting bounds on velocity thus varied both geographically and with depth.

Table 1. Nominal bounds on velocities and Poisson's ratio (σ) for the inversion as a function of model unit.

Model Unit	*Vp* (km/s)	*Vs* (km/s)	Poisson's ratio (σ)
Upper Crust	5.8 – 6.2	3.2 – 3.5	0.23 – 0.34
Middle Crust	6.1 – 6.8	3.4 – 3.8	0.24 – 0.33
Lower Crust	6.7 – 7.2	3.7 – 4.1	0.25 – 0.32
Mantle (relative to AK135)	± 0.2	± 0.1	± 0.26 – 0.31

Travel-Time Tomography for the Compressional Velocity Model

The 3D tomography method developed for this project is an extension of the method developed by Reiter et al. (2005). Forward modeling of travel times in a 3D velocity model is done with the finite-difference method of Podvin and Lecomte (1991) as implemented by Lomax et al. (2001). We extended this software with algorithms for mapping Earth models in spherical coordinates to flat-Earth, Cartesian models, as needed by the P-L algorithm, and for generating the partial derivatives (sensitivities) of the calculated travel-times with respect to the velocity model parameters.

As noted above, each iteration of our joint inversion method performs linearized tomography, (i.e. with the travel-time sensitivities held fixed). The linearized problem is solved as a regularized least-squares problem, with the regularization functional serving to constrain the size and spatial smoothness of velocity perturbations in a geostatistical sense (see above). We invoke velocity bounds with the use of a parameter mapping technique; we solve directly for an unconstrained variable that is mapped onto a finite range of velocity values. This mapping technique changes the least-squares problem from a linear to a nonlinear one, even though the forward problem is linearized. We use a *nonlinear* conjugate gradients technique to obtain the solution.

The body-wave tomography results shown at the end of the paper were obtained with the following choices for smoothing parameters. The prior standard deviation of *Vp* was set to 2% of the reference model velocity. The correlation distances were 500 km and 100 km in the horizontal and vertical directions, respectively. The velocity was allowed to vary in the crust below the sediment layers of the CRUST2.0 model and to a depth of 410 km in the mantle. No smoothing was applied across the crustal interfaces (separating upper, middle and lower crust) or across the Moho discontinuity.

Surface-Wave Inversion for the Shear Velocity Model

Forward modeling and inversion of surface-wave dispersion are each performed as two-step procedures. The following sections describe each step of these procedures.

Forward Modeling of Group Delays. Our approach for modeling surface wave dispersion in a 3D Earth employs the same approximation used by Stevens and Adams (1999), Ritzwoller and Levshin (1998) and others, which states that the phase delay, or phase travel time, between an event and a station is obtained as an integral of the local phase velocity along a travel path. Our procedure, however, uses a minimum-time path through the phase-velocity structure instead of a great-circle path, as we now describe.

We calculate phase delays in a two-step process. The first step is to compute the dispersion response for each geographic grid point of the 3D Earth model, as determined by the 1D velocity/density profile defined for each point. We perform these dispersion calculations using software adapted from a set of modal summation codes (Herrmann, 2002). Implicit in the use of these codes is an "Earth-flattening" transformation that corrects for the Earth's sphericity.

Once we have completed the dispersion calculations over the geographic grid, we collate the output from these calculations at the frequencies of interest to produce a set of phase- and group-velocity maps. The next step in the dispersion forward-modeling process is the calculation of phase-delay (or "phase-time") maps from the phase-velocity maps, using the P-L ray tracer. Surface-wave path delays are typically found by integrating along the great circle connecting the source and receiver points (Woodhouse and Dziewonski, 1984), which is correct for a 1D

Earth model in which the local dispersion is the same at each latitude and longitude. However, lateral heterogeneities in the crust and upper mantle can cause both Rayleigh and Love waves to deviate laterally relative to the great-circle path. A better approximation to phase and group travel times is found by integrating the phase and group slownesses along the minimum-time path through the frequency-specific, 2D phase velocity map. We have adapted the P-L ray-tracing technique we use in body-wave modeling to additionally obtain phase and group delays for the source-receiver paths in our group-velocity database.

For the group delay, we integrate the group velocities along the minimum phase-time ray path. In the P-L method, a ray path is represented by the sensitivities of the phase travel time to the phase velocities of cells. We compute the cell sensitivities using the same algorithm that calculates sensitivities for body-wave travel times. The sensitivities of travel times to cell slownesses are computed using recursive back-propagation of node-to-node and node-to-cell dependencies from any given receiver point (event position) toward the source (station position). Consistent with the underlying ray theory, the resulting sensitivities are concentrated along a trajectory of cells connecting the source and receiver points, and this trajectory defines the P-L version of a ray path. For example, Figure 5 displays three examples of the ray-path sensitivities (out of more than 61,000 paths) found using our forward-modeling approach. In each subplot we show both the 2D sensitivities and the great-circle path between station and event at a particular period. The results demonstrate the significant off-path deviations that can occur, even at mid-range periods.

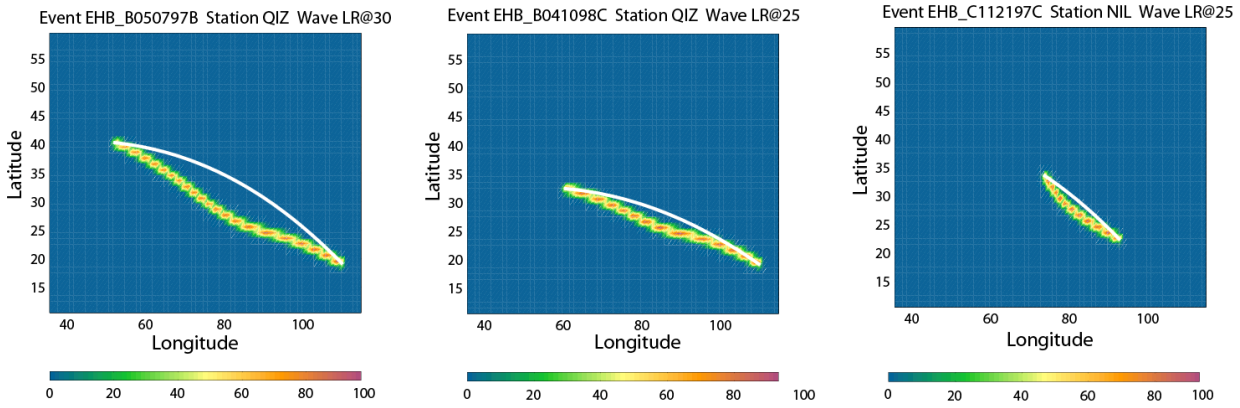

Figure 5. Examples of surface-wave ray-path sensitivities. White lines represent the great-circle path between the source and receiver for a particular period. Colored pixels show the sensitivities (or ray paths) derived by ray-tracing through a 2D phase-velocity map. Significant departures from great-circle-path travel can be seen, even for fairly short paths (right-hand subplot).

Group Velocity Tomography. To produce an updated set of group velocity maps that become the input to the 1D dispersion profile inversion, we employ the same tomography technique that is used to invert the body-wave travel times. The data are now observed group delays along particular source-receiver paths, for a set of frequencies, and the 3D model parameter is now group velocity as a function of latitude, longitude and period. The depth coordinate used in the body-wave tomography is replaced with logarithmic period, with an appropriate correlation "distance" assigned to accomplish some degree of smoothing over period (20% of the period in the results presented here). A departure from the body-wave tomography technique is that group velocity bounds were set to be two prior standard deviations from the reference model values. In other words, we did not derive the group-velocity bounds that are implied by the shear-velocity bounds for the Earth. In the results presented here, the prior standard deviation of group velocity was set to 3% of the initial model values, implying that the velocity bounds were 6% from the reference values.

A subset of the resulting group velocity maps is shown in Figure 6, for periods of 15, 25, 35, 40, 60 and 80 seconds. Comparison of our group velocity maps with those of other authors indicates good agreement on most long-wavelength features, with differences restricted to smaller-scale features and specific velocity variations.

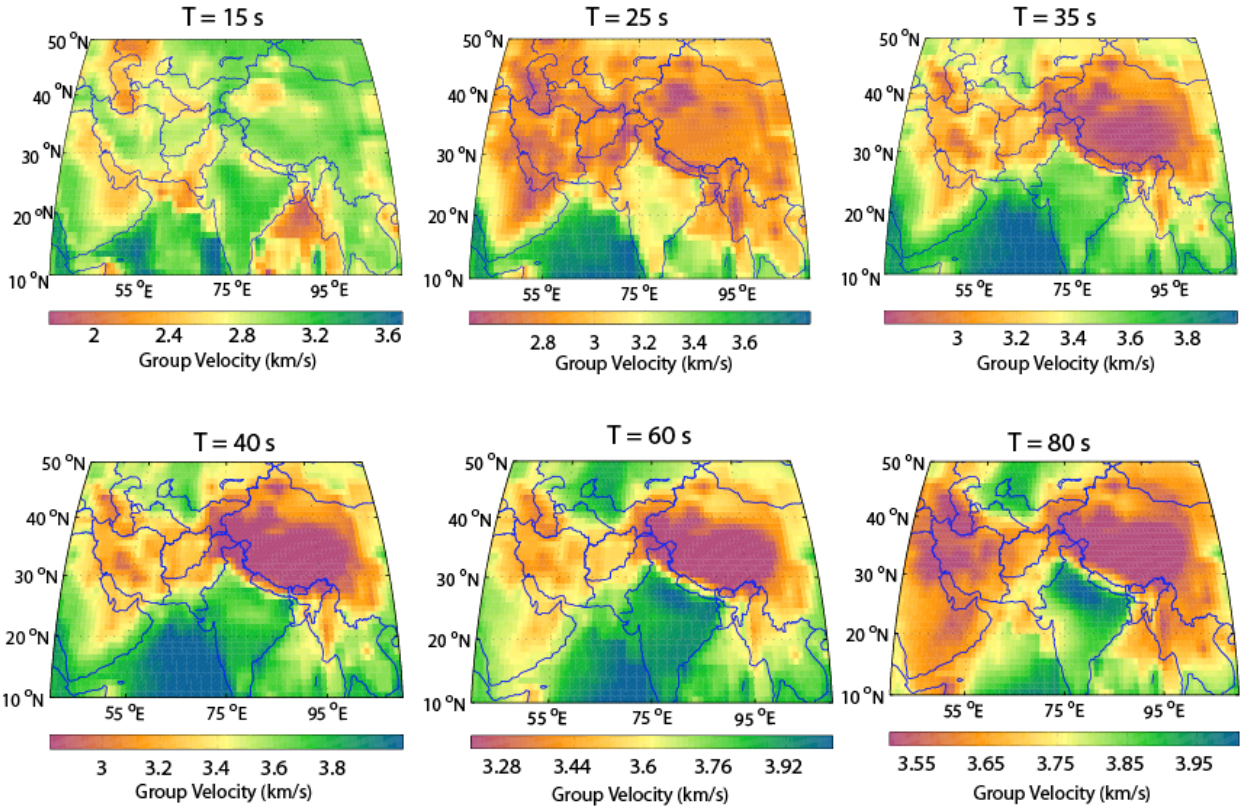

Figure 6. Results from the group velocity tomography at various periods. The results indicate strong correlation with tectonic features such as the Tibetan Plateau, Tarim Basin, continental India and the Arabian Peninsula. Note that the color maps are *not* normalized across all periods.

Dispersion Profile Inversion: Following the tomographic inversion of the group delays to retrieve a set of group velocity maps at a set of twenty-three discrete frequencies, we invert individual dispersion curves as a function of period collected from the set of group velocity maps. The result is an *S*-velocity profile as a function of depth at a single latitude and longitude point. We solve this inversion problem by minimizing a Tikhonov-regularized objective function with a bounded-value least-squares (BVLS) code (Stark and Parker, 1995). We impose upper and lower velocity bounds on the inversion, using the values described previously. We can also restrict the model to allow changes in certain 'depth zones', depending on the confidence we have in the resolving power of our data. As in the body-wave tomography, we allowed changes to the velocity model for layers in the upper, middle and lower crust, and in the upper mantle to a depth of 410 km.

Joint Inversion Results: Iteration 1

In Figure 7 we show our *Vp* and *Vs* model after completing one iteration of our joint inversion technique. Each row in the figure displays a single layer or depth horizon from the geographic model over the study region. In the top row we show the *Vp*, *Vs* and depth of the model at the top of the lower crust unit. The depth at the top of this unit varies from 8 – 40 km depth. The middle row shows the inversion results from the uppermost mantle node, corresponding to what many researchers denote the 'lid' velocity. In the bottom row of the plot, we show the velocities from a level in the model that varies from 150-174 km depth. It is interesting to note both the correlated and anti-correlated features of this model, some of which are seemingly counter-intuitive. However, without mapping the inverted *Vs* model to a prior model for the *Vp* tomography, perhaps by using a Poisson's ratio half-way between the bounds, it is difficult to determine if the models are self-consistent. These post-inversion analyses are some of the next steps to be performed before we begin to iterate the inversion.

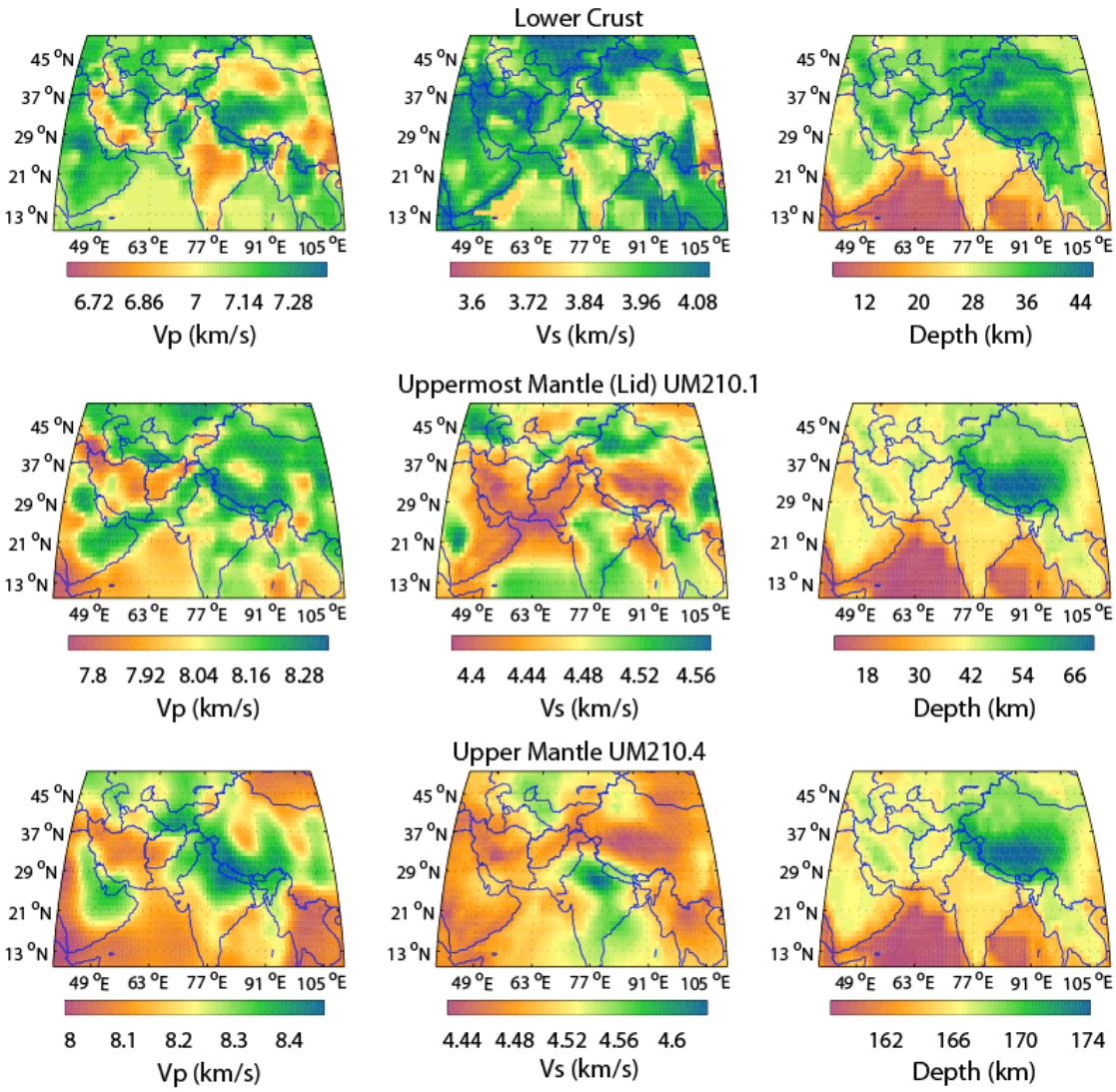

Figure 7. Compressional and shear-velocity results from the first iteration of the joint inversion method. Each row displays a nodal map of *Vp*, *Vs* and depth from the inversion model. The top row displays the result from the lower crust; middle row shows the map from the uppermost-mantle (i.e. the lid velocity); and the bottom row shows upper-mantle velocities at 150-174 km depth.

CONCLUSIONS AND RECOMMENDATIONS

In this paper we presented the basic components of our nonlinear 3D inversion algorithm, which have applied in a first-iteration step. The results appear reasonable in relation to other available models (for example, the CUB model of Ritzwoller et al. [2002]) and the known tectonics of the region. While our *Vp* and *Vs* models show some similarity, we must still evaluate the consistency of our data sets and prior velocity constraints, since we did attempt to correlate the *Vp* and *Vs* models. As we proceed to further inversion iterations, we will address these and other questions. For example, we do not know the effects of nonlinearity; that is, how strongly the ray paths will change after re-tracing them in the new model. Another factor in the nonlinearity is the potential need to relocate the earthquakes in the travel-time tomography. These issues, among others, will be addressed prior to completion of the inversion model.

Once we have developed a final model, we will validate it by relocating a ground-truth (GT) database of explosions and shallow earthquakes in the region (Bondár, Engdahl, et al., 2004) and comparing the travel-time predictions for the arrivals in the database. In addition, we will perform full-waveform modeling for paths of interest in the region to determine the goodness-of-fit for both the body and surface waves to our new joint compressional and shear-wave velocity model.

ACKNOWLEDGEMENTS

We gratefully acknowledge the contribution of the surface-wave dispersion data sets provided by the CUB and LLNL groups. Some of the figures in the paper were created using the Generic Mapping Tools (Wessel and Smith, 1991; 1995).

REFERENCES

Bassin, C., G. Laske and G. Masters (2000). The Current Limits of Resolution for Surface Wave Tomography in North America, *EOS Trans AGU*, 81, F897.

Bondár, I., E. R. Engdahl, X. Yang, H. A. A. Ghalib, A. Hofstetter, V. Kirichenko, R. Wagner, I. Gupta, G. Ekström, E. Bergman, H. Israelsson and K. McLaughlin (2004). Collection of a reference event set for regional and teleseismic location calibration, *Bull. Seism. Soc. Amer.*, 94, 1528-1545.

Bondár, I., S. C. Myers, E. R. Engdahl, and E. A. Bergman (2004). Epicentre accuracy based on seismic network criteria, *Geophys. J. Int'l*., 156, 483-496.

Engdahl E. R., R. van der Hilst, and R. Buland (1998). Global teleseismic earthquake relocation with improved travel times and procedures for depth determination, *Bull. Seism. Soc. Amer.*, 88, 722-743.

Herrmann, R. B. (2002), *Computer Programs in Seismology*, Version 3.20, St. Louis University.

Kennett, B. L. N., and E. R. Engdahl (1991). Travel times for global earthquake location and phase identification, *Geophys. J. Int*., 105, 429-465.

Kennett, B. L .N. Engdahl, E. R., and Buland R. (1995). Constraints on seismic velocities in the Earth from travel times, *Geophys. J. Int'l.*, 122, 108-124.

Lomax, A., A. Zollo, P. Capuano, and J. Virieux (2001). Precise, absoute earthquake location under Somma-Vesuvius volcano using a new 3D velocity model, *Geophys. J. Int'l.*, 146**,** 313-331.

Podvin, P., and I. Lecomte (1991). Finite difference computation of travel times in very contrasted velocity models: a massively parallel approach and its associated tools, *Geophys. J. Int.*, 105, 271-284.

Reiter, D., W. Rodi, and M. Johnson (2005). Development of a tomographic upper-mantle velocity model beneath Pakistan and northern India for improved regional seismic event location, *Bull. Seis. Soc. Amer.*, 95, 926-940.

Ritzwoller, M. H., and A. L. Levshin (1998). Eurasian surface wave tomography: Group velocities, *J. Geophys. Res.,* 103, B3, 4839-4878.

Ritzwoller, M. H., N. M. Shapiro, M. P. Barmin and A. L. Levshin (2002). Global surface wave diffraction tomography, *J. Geophys. Res*., 107**,** doi: 10.1029/2002JB001777.

Rodi, W., C. A. Schultz, G. Johannessen, and S. C. Myers (2005). Grid-search location methods for ground-truth collection from local and regional seismic networks, *Final Technical Report* to National Nuclear Security Administration, Dept. of Energy, Contract Nos. DE-FC03-01SF22397 and W-7405-ENG-48.

Stark, P. B. and R. L. Parker (1995). Bounded-variable least-squares: an algorithm and applications, *Comput. Stat.*, 10, 129-141.

Stevens, J. L., and D. A. Adams (1999). Improved surface wave detection and measurement using phase-matched filtering and improved regionalized models, in the *Proceedings of the 21st Annual Seismic Research Symposium*, Las Vegas, NV, 274-282.

Tikhonov, A. N., and V. Y. Arsenin (1977). *Solutions of Ill-Posed Problems*, Winston & Sons, Washington, DC.

Wessel, P., and W. H. F. Smith (1991). Free software helps map and display data, *Eos Trans. AGU*, 72, 441, 445-446.

Wessel, P., and W. H. F. Smith (1995). New version of the Generic Mapping Tools released, *Eos Trans. AGU*, 76, 329.

Woodhouse, J. H., and A. M. Dziewonski (1984). Mapping the upper mantle: three-dimensional modeling of Earth structure by inversion of seismic waveforms, *J. Geophys. Res*., 89, 5953-5986.